Published in final edited form as:
J Am Chem Soc. 2008 November 19; 130(46): 15348–15360. doi:10.1021/ja8033312.

Modulation of the Ligand-Field Anisotropy in a Series of Ferric Low Spin Cytochrome *c* Mutants derived from *Pseudomonas aeruginosa c*-551 and *Nitrosomonas europaea c*-552. An NMR and EPR Study

Giorgio Zoppellaro[‡], **Espen Harbitz**[‡], **Ravinder Kaur**[§], **Amy A. Ensign**[§], **Kara L. Bren**[§,*], and **K. Kristoffer Andersson**[§,*]

‡*Department of Molecular Biosciences, University of Oslo, PO Box 1041 Blindern, Oslo NO-0316, Norway*

§*Department of Chemistry, University of Rochester, Rochester, New York 14627-0216, USA*

Abstract

C-type cytochromes with histidine-methionine (His-Met) heme axial ligation play important roles in electron-transfer reactions and in enzymes. In this work two series of cytochrome *c* mutants derived from *Pseudomonas aeruginosa* (Pa *c*-551) and from the ammonia oxidizing bacterium *Nitrosomonas europaea* (Ne *c*-552) were engineered and over-expressed. In these proteins, point mutations were induced in a key residue (Asn64) near the Met axial ligand that have a considerable impact on both heme ligand-field strength and on the Met orientation and dynamics (fluxionality), as judged by low-temperature electron paramagnetic resonance (EPR) and nuclear magnetic resonance (NMR) spectra. The Ne *c*-552 has a ferric low spin (S=1/2) EPR signal characterized by large *g* anisotropy with g_{max} resonance at 3.34; a similar large $g_{\mathbf{max}}$ value EPR signal is found in the mitochondrial Complex III cytochrome c_1. In Ne *c*-552, deletion of Asn64 (NeN64Δ) changes the heme ligand-field from more axial to rhombic (small *g* anisotropy and g_{max} at 3.13) and furthermore hinders the Met fluxionality present in the wild-type enzyme. In Pa *c*-551 (g_{max} at 3.20) replacement of Asn64 with valine (PaN64V) induces a decrease in the axial strain (g_{max} at 3.05) and changes the Met configuration. Another set of mutants prepared by insertion (ins) and/or deletion (Δ) of a valine residue adjacent to Asn64, resulting in modifications in the length of the axial Met-donating loop (NeV65Δ, NeG50N/V65Δ, PaN50G/V65ins), did not result in appreciable alterations of the originally weak (Ne *c*-552) or very weak axial (Pa *c*-551) field, but had an impact on Met orientation, fluxionality and relaxation dynamics. Comparison of the electronic fingerprints in the over-expressed proteins and their mutants reveals a linear relation between axial strain and average paramagnetic heme methyl shifts, irrespective of Met orientation or dynamics. Thus, for these His-Met axially coordinated Fe(III) the large $g_{\mathbf{max}}$ value EPR signal does not represent a special case as is observed for bis-His axially coordinated Fe(III) with the two His planes perpendicular to each other.

Keywords

Cytochrome *c*; EPR; NMR; ligand-field anisotropy; point mutation

*To whom correspondence should be addressed: K. Kristoffer Andersson, k.k.andersson@imbv.uio.no, Phone: +47-22856625 Fax: +47-22856041, Kara L. Bren, bren@chem.rochester.edu Phone: +1-585-2754335 Fax: +1-585-2760205

INTRODUCTION

The class of cytochrome *c* (cyt *c*) proteins is a diverse group of heme-containing electron-transfer proteins known to play key roles in biological processes such as respiration and photosynthesis.[1] Cyt *c* contains a heme prosthetic group (iron protoporphyrin IX) which is covalently bound to the protein backbone through two (in some cases one) thioether bonds made by cysteine residues.[2] In class I cyts *c* histidine (His) and methionine (Met) form the fifth and sixth axial ligands for the caged heme iron. The constrained structural environment of the heme group forces the iron ion to adopt a low-spin electronic configuration in both the oxidized (Fe^{3+}, S = 1/2) and reduced (Fe^{2+}, S = 0) states.[3] Within the conserved heme binding motif Cys-X-X-Cys-His, His serves as a heme axial ligand and is structurally constrained, such that its orientation can be considered close to be rigid and typically aligned along the heme α-γ-meso axis.[4,5] All together these structural features of the heme core and its surroundings contribute to minimizing the reorganization energy required for electron transfer.[6] Active research in the field aims to understand the correlations between protein structure, physical/chemical properties and biological function. In this framework, the complementary use of electron paramagnetic resonance (EPR), nuclear magnetic resonance (NMR) and Mössbauer spectroscopy allows the unveiling of the electronic configuration of the Fe^{3+} heme ion, axial ligands' nature and dynamics and the protein's structural stability, i.e. the factors contributing to determine protein function.[7-9] In this work is described a spectroscopic study carried out on two series of mutants of *Pseudomonas aeruginosa* cytochrome *c*-551 (Pa *c*-551) and, from the ammonia oxidizing bacterium, *Nitrosomonas europaea* cytochrome *c*-552 (Ne *c*-552) using ^{1}H NMR and X-band EPR techniques. The aim is to investigate whether point mutations in key residues near the heme axial methionine modify the heme ligand-field strength.

The cytochromes Pa *c*-551 and Ne *c*-552 are very similar to each other.[10] They are small (8.7 kDa for Pa *c*-551 and 9.1 kDa for Ne *c*-552), soluble, monomeric proteins, with a high α-helical content (four helices), a similar polypeptide fold, and positive reduction potentials (+291 mV for Pa *c*-551[11] and +250 mV for Ne *c*-552[5]). Biologically Pa *c*-551 acts as an electron donor for cytochrome cd_1 in nitrite and nitrate respiration,[12-14] with a function analogous to that known for mitochondrial cytochrome *c*, which is part of the respiratory chains of eukaryotic organisms.[15] The three-dimensional structure of Pa *c*-551 is known by both X-ray crystallography and solution NMR (Figure 1A).[16,17] Similarly, Ne *c*-552 is involved in several physiological reactions such as acting as an electron donor to the terminal cytochrome oxidase[18] and to a diheme peroxidase,[19] or as electron acceptor from the tetraheme cytochrome *c*-554;[20] its three-dimensional structure is known by solution NMR studies (Figure 1B).[5] The strong structural homology and the long consensus in the amino acid sequence between Ne *c*-552 and Pa *c*-551 allow the sequence of Ne *c*-552 to be denoted by using the same numbering scheme employed for the corresponding analogous residue in Pa *c*-551, hence in Ne *c*-552 the number 3 is assigned to the N-terminal residue Asp3. An asparagine residue (Asn64), close in space to Met61 and located on the axial methionine-bearing loop in these proteins might interact with the sulphur atom of the axial ligand Met61.[5, 16-17] This interaction in addition to steric effects has been shown to play an important role in determining the axial methionine conformation relative to the heme in Pa *c*-551.[21] Moreover in Pa *c*-551 there is a hydrogen bond between Pro25 (CO) and the axial ligand His16 (NπH) which is conserved in Ne *c*-552, with an hydrogen-acceptor distance of 1.81 Å. This interaction may contribute to constraining the orientation of the imidazole ring with respect to the heme plane.

Although Pa *c*-551 and Ne *c*-552 bear many similarities in structure and heme axial ligation, the spectroscopic fingerprints of the heme groups in these two proteins are strikingly different, as evidenced by NMR spectroscopy of the paramagnetic ferric proteins[21-23] and low-temperature EPR studies.[24-26] The EPR spectra of low-spin cyt *c* with the $(d_{xy})^2(d_{xz})^2(d_{yz})^1$ electronic configuration can exhibit a distinct set of *g*-resonances, grouped in two main

categories called Type I and Type II heme, according to the nomenclature introduced by Walker.[27] The relative order of energy levels of the d-orbitals of the low spin Fe^{3+} metal ion is depicted graphically in Figure 2.[26-28] In Type II heme all three *g* values (g_{max}, g_{mid} and g_{min}) can be resolved in the spectra and characterized by small *g*-anisotropy ($g_{max} < 3.2$). This situation is encountered in Pa *c*-551 as it exhibits signals at 3.20 (g_{max}), 2.06 (g_{mid}), and 1.23 (g_{min}) (*vide infra*). Type I hemes exhibit much larger *g*-anisotropy, with $g_{max} > 3.3$ and g_{mid}, g_{min} rather small and broad.[29-31] The g_{min} component in these spectra is often so weak that it becomes, in most cases, difficult to detect. This situation is seen in the EPR envelope of Ne *c*-552 with signals at 3.34 (g_{max}), 1.87 (g_{mid}), and a very weak and broad *g*-resonance at 1.17 (g_{min}). Such *g*-values assignments have been furthermore supported by previous Mössbauer spectra simulations.[25] These two different types of magnetic behaviors imply the occurrence of two distinct ground state configurations for the low-spin Fe^{3+} ion; one characterized by near-degeneracy between d_{xz} and d_{yz} orbitals with energy difference ΔE (with $\Delta E = E(d_{yz}) - E(d_{xz})$) smaller than the spin-orbit coupling constant (ξ), and the other one featuring a large ΔE between the d_{xz} and d_{yz} orbitals, at least two or three times ξ (Figure 2). Low-spin heme proteins having large *g*-anisotropy and large g_{max} signals[32] (Type I) are also referred to as highly anisotropic low-spin heme[29] or highly axial low-spin heme (HALS)[31,33] and those exhibiting small *g*-anisotropy and rather small g_{max} (< 3.2) (Type II) are also referred to as rhombic heme. According to present knowledge, the HALS envelope arises when the ligand-field geometry around the Fe^{3+} ion is perturbed in such a way that the heme group is subjected to large axial (Δ) strain and a relatively weak rhombic field component (*V*) generated by the axial ligands.[31, 34-36] In the limiting case of a pure axial system, the rhombic field component *V* would vanish (~0), while g_{max} would approach the value of 4 and g_{mid}, g_{min} would approach 0.[2, 31,37] Thus the heme core, depending on the strength of the rhombic versus axial field (V/Δ), can experience the whole spectrum of intermediate axial-strain configurations, assuming that the limiting ratio $0 < V/\Delta < 0.67$ is satisfied.[2,27]

The correlations between the observed EPR axial strain and axial ligand arrangements have been extensively investigated and well rationalized for *b*-type cytochromes with bis-histidine heme axial ligation[27] and their mimicking complexes.[38] The two histidine ligands coordinating the heme iron in these systems are both orthogonal to the heme plane. When the two axial ligands lie in perpendicular planes the HALS EPR signal is observed, and if the axial ligands adopt a parallel orientation, the resulting EPR signal is much more rhombic.[39,40] From these studies, correlation of structure with the observed electronic properties of the heme group shows that the presence of strong axial ligands (strong σ-donors and weak π-acceptors), a highly saddled-shaped heme plane, and/or electron withdrawing substituents at the meso positions of the porphyrin cause the heme configuration to be stabilized towards the axial $(d_{xy})^2(d_{xz},d_{yz})^3$ state. For cytochromes *c* with a methionine (Met) and histidine (His) coordinated to heme iron, a clear assessment of the leading factors that steer the ligand-field strength is still rather unclear. Several biologically important cytochromes *c* showing large g_{max} values and large *g* anisotropy can be found in literature; these include for example the mitochondrial cytochrome c_1 from Complex III ($g_{max} = 3.37$),[31,41] the thiosulfate-oxidizing enzyme SoxAX ($g_{max} = 3.50$),[42] the di-heme cytochrome *c*-553 peroxidase from *Nitrosomonas europaea* ($g_{max} = 3.38$)[19] and a cytochrome *c*-553 from *Bacillus pasteurii* with a known high resolution 3D structure ($g_{max} = 3.36$).[25,43] Ne *c*-552 can serve as a model for this class of proteins with large g_{max} values.

The EPR and NMR analyses performed on our series of mutants of Pa *c*-551 and Ne *c*-552 discloses that the ligand-field can be shifted from weakly axial (Pa *c*-551) or moderately axial (Ne *c*-552) to nearly rhombic (PaN64V and NeN64Δ) by mutating residues near the heme axial methionine. This effect is proposed to result from both steric factors and perturbation of the electrostatic (polar) interaction between the axial ligand Met61 and Asn64 (N64). Substitution of N64 with a group having similar polarity but slightly greater bulk such as glutamine

(PaN64Q) only slightly modifies the original ligand-field witnessed in the wild type form. The same is true for NeV65Δ, where the axial methionine-bearing loop has been shortened by a valine residue. These mutants do however exhibit differences in the heme relaxation properties and in the Met fluxionality relative to wild-type proteins, thus minor modifications of the Fe-Met interaction are shown to tune the systems to lower (rhombic) symmetries.

MATERIALS AND METHODS

Protein Expression and Purification

The pSNEC (Amp^r) plasmid[10] containing the Ne *c*-552 gene proceeded by an *E. coli*-compatible signal sequence was used as a template for site-directed mutagenesis and for expression of Ne *c*-552 and mutants NeN64Δ and NeG50N/V65Δ. NeV65Δ was prepared as described.[44] The NeN64Δ deletion mutant was prepared by the Megawhop method[45] using the primer 5′-CCAATGCCGCCAGTGAACGTGAG-3′. NeG50N/V65Δ was prepared using the pSNECV65Δ plasmid[44] as a template and the QuickChange mutagenesis method with *PfuUltra* DNA polymerase (Stratagene) using the following primer: 5′-CTGGCAGGTAAAATCAAAAACGGCAGCAGCGGT-3′. Parental methylated DNA was digested with *Dpn*I, and the products were transformed into XL1-Blue supercompetent cells. Expression and purification of Ne *c*-552 variants was as described for Ne *c*-552.[10] The pETPA plasmid (Amp^r)[23] containing the Pa *c*-551 gene proceeded by a signal sequence was used as a template for site-directed mutagenesis and for expression of Pa *c*-551 and mutants PaN64V and PaN50G/V65ins. PaN64V and PaN50G/V65ins were prepared using the Megawhop procedure as described above with the following primers: 5′-GCCGCCGGTCGCGGTCAGCGA-3′ and 5′-GCGGATCAAGGGCGGCAGCCA-3′, respectively. The preparation of PaN64Q was as previously reported,[21] and expression and purification of PaN64V and PaN50G/V65ins was as described for recombinant wild-type Pa *c*-551.[23] DNA sequencing confirmed the results of all mutations. NeV65Δ and NeG50N/V65Δ were found to have two additional mutations: R33K and N36D. These conservative mutations occur in a flexible surface loop and are not expected to have a significant impact on the fold of the proteins.

NMR Spectroscopy

^{1}H NMR spectra were collected on a Varian INOVA 500-MHz spectrometer. Samples were 2-3 mM in protein (NeN64Δ, NeV65Δ, NeG50N/V65Δ, PaN64V, or PaN50G/V65ins) in 50 mM sodium phosphate buffer, pH 7.0 (10% D_2O). A 5-fold molar excess of $K_3[Fe(CN)_6]$ was present to maintain samples in the oxidized state. 2-D NOESY (mixing time 100 ms) and TOCSY (spin-lock time 50 ms) spectra were collected with 8192 points in the F2 dimension, 512 increments in the F1 dimension, and a 30,000-Hz spectral width. Chemical shifts for heme methyl ^{1}H resonances of oxidized NeN64Δ, NeV65Δ, NeG50N/V65Δ, PaN64V, and PaN50G/V65ins were determined by identifying NOESY connectivities between heme substituents, and between heme substituents and nearby amino acids. Assignments for Pa *c*-551,[22,23] PaN64Q,[21] and Ne *c*-552[10,22] are available in the literature.

EPR Spectroscopy

The EPR measurements for the wild type forms and mutants of cytochrome *c* from *Pseudomonas aeruginosa* and *Nitrosomonas europaea* (protein concentration 210-310 μM, 50 mM HEPES, pH 7.5) were acquired with a dual-band X-cavity on a Bruker Elexsys 500E spectrophotometer characterized by a cavity quality factor (*Q*) 3800-4200 within the measurements and equipped with a He-flow cryostat (ESR 900, Oxford Instruments). The XSophe (ver. 1.1.3) EPR simulation platform and XeprView (ver. 1.2b.33) software were provided by Bruker.[44] The protein samples were prepared by employing fast freezing procedures, down to 77 K, of the initial protein solution placed in the EPR tube kept at 0 °C.

Slow freezing (5 min) at -30 °C in an ethanol bath followed by cooling at 77 K in liquid nitrogen or annealing always produced broader and less resolved EPR envelopes once the samples have been measured at cryogenic temperatures (See Supporting information). In particular we noticed that slow cooling and annealing induced enhanced signals of the copper (Cu^{2+}) impurity (around g ~ 2) compared to the EPR resonances obtained with faster sample cooling. The EPR spectra were baseline corrected upon subtraction of the cavity background and the EPR tube containing buffer (keeping the same filling volume) recorded under identical conditions. In all the measurements for the cytochromes *c*, both wild type forms and mutants, the EPR signals were too broad to detect above 30 K, thus most of the EPR spectra were collected at 10 K. In addition, in most of the expressed mutants, the g_{max} EPR signal intensities (I) of the anisotropic *g*-tensors followed the Curie-law (I = C/T) within the temperature range examined, with a linear increase upon decreasing the sample temperature (T), with the exception of one mutant (NeG50N/V65Δ) where (I) deviated from linearity.

Correlation between EPR g-tensor values and ligand-field parameters

The ligand-field correlation analysis, based on the formalism introduced by Griffith[34,36] and developed by Taylor[35] has been used to extract the V/ξ (rhombic) and Δ/ξ (axial) ligand field terms. Axial and rhombic terms correlate with the *g*-tensor values as seen by the following equations:

$$\frac{V}{\xi}=\frac{E_{yz}}{\xi}-\frac{E_{xz}}{\xi}=\frac{g_{xx}}{g_{zz}+g_{yy}}+\frac{g_{yy}}{g_{zz}-g_{xx}} \quad (1)$$

$$\frac{\Delta}{\xi}=\frac{E_{yz}}{\xi}-\frac{E_{xy}}{\xi}-\frac{V}{2\xi}=\frac{g_{xx}}{g_{zz}+g_{yy}}+\frac{g_{zz}}{g_{yy}-g_{xx}}-\frac{V}{2\xi} \quad (2)$$

Eq 1 and eq. 2 are valid as long as the following normalization condition holds: [35,49]

$$g_{xx}{}^2+g_{yy}{}^2+g_{zz}{}^2+g_yg_z-g_xg_z-g_xg_y-4\left(g_{zz}+g_{yy}-g_{xx}\right)=0 \quad (3)$$

Eq. 3 can be used to calculate the third *g* value when only two *g* terms are measurable. The complication hidden in eq. 3 is that the EPR measurements can provide only the magnitude but not the signs of the *g*-tensor values (either positive or negative). One constraint is to consider that the sum [$g_{zz} + g_{yy} - g_{xx}$] should be positive.[27] This condition limits the number of possible choices for the signs of *g*. In the correlation analyses performed in this work all three *g* values have been assumed to be positive. Eq. 3 fails when residual contributions from higher excited states are not negligible, in the absence of efficient spin-orbit mixing among the t_{2g} orbitals or when the system adopts a $(d_{xz},d_{yz})^4(d_{xy})^1$ electronic configuration.[45]

RESULTS AND DISCUSSION

^{1}H NMR Spectra of Oxidized Protein Variants

Ferricytochromes *c* with His-Met heme axial ligation display diverse patterns of hyperfine-shifted resonances in ^{1}H NMR spectra. This variation results primarily from differences in the axial Met orientation relative to the heme group.[46,47] For the common rhombic configuration, as shown in Figure 2, the electronic interaction of the d_{xz}, d_{yz} iron orbitals with the filled π-porphyrin orbitals $3e_g(\pi_{x,y})$[26,48] allows delocalization of the unpaired spin toward the heme pyrroles, in agreement with both Hückel[47] and density functional (DFT)[49,50] calculations.

The estimated main components of the Highest Occupied Molecular Orbital (HOMO) in the d^6 low-spin electronic configuration (Fe^{2+}, with His and Met as axial ligands) contain gross atomic population of d_{xy} (65.4%), d_{xz} (10.5%) and d_{yz} (9.3%) with negligible contribution from d_{x2-y2} and d_{z2} orbitals (both under 0.1%).[49] Hence the HOMO has mainly metal character. Similarly, a dominating metal character occurs in the SOMOs (Singly Occupied Molecular Orbital) when the heme adopts the low-spin d^5 electronic configuration (Fe^{3+}). Here the electronic ground state has been found to be a doublet (S = 1/2) state with a low-lying excited quartet (S = 3/2) state (ΔE_{dq} = 594.5 cm^{-1}).[50] Interaction of the SOMO with the π-system of the porphyrin core, which possesses approximate D_{4h} symmetry, must involve molecular orbitals of the porphyrin having e_g symmetry under D_{4h}.[51,52] As a result, the chemical shifts of the porphyrin substituents (i.e. the heme methyl groups at positions 1, 3, 5, and 8 in Figure 3) are dominated by the Fermi contact contribution to the hyperfine shift.[47,53] Depending on the orientation of the heme axial Met (and His), spin density is directed primarily towards the $3e_g(\pi_x)$ or $3e_g(\pi_y)$ orbital, yielding a large spread (~20 ppm) of heme methyl shifts.[47,54,55] Two prototypical patterns of heme methyl shifts corresponding to the two most frequently observed axial Met orientations can be observed. In what will be referred to herein as orientation A (Figure 3A), which is seen in Pa *c*-551, the heme axial Met ε-CH_3 is directed toward pyrrole IV. This type of arrangement causes the unpaired electron to be localized more to pyrroles I and III ($3e_g(\pi_y)$) rather than to pyrroles II and IV ($3e_g(\pi_z)$), yielding a heme methyl shift arrangement of 5-CH_3 > 1-CH_3 > 8-CH_3 > 3-CH_3 (5183, hereafter). Orientation B, in which the axial Met ε-CH_3 is directed toward pyrrole I, as is observed in the mitochondrial cytochromes *c*, displays a 8-CH_3 > 3-CH_3 > 5-CH_3 > 1-CH_3 (8351) heme methyl shift pattern. In Ne *c*-552, however, the methyl shift spread is unusually small, only 4.2 ppm, indicating nearly equal unpaired electron spin-density at the four pyrrole groups.[10,22] Furthermore Ne *c*-552 exhibits rapid fluxionality of the heme axial Met on the NMR time scale, while such an effect is absent in Pa *c*-551.[10] The compressed heme methyl shift pattern for Ne *c*-552 is consistent with the averaging of the shifts for the two prototypical Met conformations (Figure 3C).[9] Evidence for the existence of Met fluxionality also is provided by the line broadening shown by the heme methyl resonances of Ne *c*-552 at low temperature and is consistent with the presence of a chemical exchange process impacting the heme methyl shifts.

The factors controlling Met fluxionality are yet uncertain, although mutation of amino acid residues interacting with the heme axial Met have been shown to suppress or induce Met dynamics, as well as alter Met orientation.[53,56,57] A suggested hypothesis is that a weak Fe-Met bond combined with a large heme pocket that can accommodate multiple Met orientations results in Met fluxionality.

The patterns and temperature-dependent line widths of the heme methyl resonances in NMR provide information on the orientation and dynamics of the heme axial Met. However, the relationship between the magnitudes of axial and rhombic distortions (and thus the EPR *g*-values) and His/Met ligand orientation is less clear. A number of cytochromes and model hemes with bis-histidine axial ligation display HALS-type EPR spectra, as a result of a mutual perpendicular orientation of the axial imidazole ligands (intra-ligand plane angle ~70° - 90°) resulting in a small value of V/ξ. Hemes with an angle between two axial imidazole planes of less than 70° display rhombic EPR spectra.[38] Any correlation between EPR spectra and orientations of the ligands in His/Met-ligated heme, however, has not yet been found. For example, the mitochondrial cytochromes *c* have an intra-ligand angle (measured as the angle between the π nodal planes of the His and Met) of ~48° and display rhombic EPR spectra (g_{max} ~ 3.1).[58] Pa *c*-551, with an intra-ligand angle of ~54°, has a more axial EPR spectrum with g_{max} of 3.2.[26] However, the axial His and Met orientations for *Bacillus pasteurii* cytochrome *c*-553 are similar to those of the mitochondrial cytochromes *c* (with an intra-ligand angle of ~ 48°)[43], but this protein exhibits a large g_{max} of 3.36.[25] Variations in effective His and Met ligand-field strength has been proposed in the analysis of ligand orientation

dependence of heme hyperfine shifts and such a phenomenon may account for the poor correlation between EPR spectra and ligand orientation in His/Met ligated hemes as well.[51]

Here, to investigate how heme axial Met orientation relates to EPR envelopes in cytochrome *c*, mutants of Ne *c*-552 and Pa *c*-551 predicted to perturb the fixed Met-Fe interaction were prepared.[4,59] The mutants were made by modifying the sequence in the loop containing the axial methionine. Two deletion mutants of Ne *c*-552 (NeN64Δ and NeV65Δ) were expressed to give variants with a loop of the same length as that present in Pa *c*-551. Ne *c*-552 has one more residue in this loop, and the greater length of this loop is proposed to alter its packing against the heme,[5] which may contribute to the observed Met fluxionality in Ne *c*-552. The double mutant NeG50N/V65Δ additionally substitutes the flexible G50 residue at the end of the loop with asparagine, the corresponding residue in Pa *c*-551. The complementary double mutant of Pa *c*-551 (PaV65ins/N50G) was additionally prepared together with the PaN64V mutation which replaces the polar asparagine residue with a hydrophobic, isosteric group. The downfield region of the ^{1}H NMR spectra of the resulting mutants and the corresponding wild-type proteins in the oxidized state are shown together in Figure 4, with key results summarized in Table 1. Mutation of N64 to V in Pa *c*-551 changes the heme methyl shift pattern from 5183 to 8351 (Figure 4A, configuration B in Figure 3). PaN64V also displays line broadening in the heme methyl resonances as temperature is lowered (data not shown), suggesting the occurrence of dynamics in the axial Met. Unlike the over-expressed Ne *c*-552, however, the heme methyl shifts are not compressed, indicating a predominant B configuration for the Met orientation. Deletion of N64 in Ne results in an increase in the spread of heme methyl shifts with a 8351 heme methyl shift pattern, consistent with Met in orientation B (Figure 4C, 4D). As temperature is lowered, the NMR spectrum of this mutant shows no evidence of line broadening. A shoulder is detected on the high-field side of the heme 3-CH_3 resonance in NeN64Δ. Inspection of the NOESY spectrum allows assignment of the shoulder to the 3-CH_3 resonance of a minor conformer. The small difference in chemical shift from the major form indicates the minor conformer has a Met orientation nearly identical to that of the major conformer and thus does not indicate fluxionality of the Met which involves a significant reorientation of Met. The minor conformation may arise from heterogeneity in the polypeptide conformation near the 3-CH_3, as has been observed in horse cytochrome *c*.[60] In conclusion, this mutation fixes the axial Met position under these experimental conditions. In contrast, the NeV65Δ mutant shows minimal difference from Ne *c*-552 in the heme methyl resonances (Figure 4E), and it also displays line broadening at low temperature indicating that the Met maintains fluxionality as observed in the correspondent wild-type. The double mutant NeG50N/V65Δ, however, takes on a 5183 pattern and shows no evidence of line broadening over the temperature range studied. Such behavior suggests a Met fixed in orientation A (Figure 4F). Although the narrow chemical shift range shown by NeG50N/V65Δ is suggestive of Met fluxionality, but as linebroadening is not observed for this mutant, we tentatively assign the Met orientation as A. Like NeN64Δ, NeG50N/V65Δ displays evidence of population of a minor conformer that is very similar to the major form in the presence of a small peak on the low-field side of the heme 1-CH_3 resonance that can be assigned to 1-CH_3 in a minor conformation. The corresponding PaN50G/V65ins ("ins" indicating 1-residue insertion) mutant maintains the 5183 pattern of Pa *c*-551, but shows line broadening consistent with Met dynamics (Figure 4G). Thus, a whole range of behaviors of the heme axial Met (fixed in orientation A or B, or fluctuating between these two orientations) is observed in these variants. Previously published results on the axial Met orientation and dynamics of variants derived from Pa *c*-551 are additionally reported in Table 1 for comparison together with data for other cytochromes. In order to quantify the perturbation of the heme ligand-field induced by point mutation and to complement the analyses of the NMR methyl paramagnetic shifts,[61] low temperature EPR studies were performed and the results are presented below.

Ligand-field analyses of cytochrome c-551 from Pseudomonas aeruginosa and its perturbation upon point mutation

The EPR spectrum of the *E. coli* overexpressed wild-type Pa *c*-551 is shown in Figure 5A. The three *g*-tensor resonances fall at g_{max} = 3.20(1), g_{mid} = 2.06(2), and g_{min} = 1.23(2) and, noticeably, these values confirm the earlier conclusion made by Gadsby and Thomson[26] that Pa *c*-551 is a very weak axial system, where $V = 1.28(2)\xi$ and $\Delta = 3.45(3)\xi$ (with ξ = 400 cm^{-1}).[27] In PaN64V, replacement of the asparagine that interacts with the axial ligand Met61 with a valine changes the Met orientation from A to B. As shown in Figure 5B, the three *g*-tensor values were observed in the PaN64V EPR spectrum. Although its g_{min} component was broader ($\Delta\nu \sim$ 60 mT) than the same g_{min} resonance observed in Pa *c*-551, its breadth did not hinder clear determination of all three *g* values at 3.05(1) (g_{max}), 2.23(2) (g_{min}) and 1.31(3) (g_{mid}). The derived ligand field parameters, *V* (rhombic) and Δ (axial) (see also Table 2), fall respectively at $V = 1.53(2)\xi$ and $\Delta = 2.80(5)\xi$, which gives a V/Δ of 0.55, hence a stronger rhombic field acts on the Fe^{3+} heme group so that it adopts lower symmetry. In order to determine whether Met fluxionality observed by NMR correlates with EPR parameters, the mutant PaN64Q which exhibits Met fluxionality[21] was probed. The resulting EPR envelope for this mutant is shown in Figure 5C. Even though only one clear resonance could be detected in the spectrum at 3.21(1) (g_{max}), this resonance resembles the g_{max} term observed in Pa *c*-551. Because of the strong Cu^{2+} signal around $g \sim$2.0, only an estimate of g_{mid} can be extracted from the spectrum (2.09 ± 0.03) while the g_{min} component was poorly observed, because too broad and at high-field ($g < 1.2$). Thus we calculated a $g_{min} = 1.15 \pm 0.05$ from eq. 3 and its EPR envelope simulation. The estimated *g*-anisotropy for this mutant shows that the heme group exhibits similar crystal-field terms ($V/\Delta \sim$ 0.41) as those observed in the wild-type Pa *c*-551. The NMR spectrum of the double mutant PaN50G/V65ins indicates a minor perturbation of the axial Met-iron interaction relative to wild-type, and the resulting EPR envelope (Figure 5D) reveals only a slight decrease of ligand-field symmetry compared to Pa *c*-551, and resonances at g_{max} = 3.18(1), g_{mid} = 2.11(2), and g_{min} = 1.26(1), with $V = 1.34(2)\xi$, $\Delta = 3.31(3)\xi$ and $V/\Delta = 0.40$. The reported series of Pa *c*-551 mutants clearly demonstrates the relevance of the axial Met-bearing loop including residue N64 on raising the Fe^{3+} ligand-field symmetry and how modifications in the second coordination sphere of the heme group can trigger alteration of the heme ligand-field.

Ligand-field analyses of cytochrome c-552 from Nitrosomonas europaea and its perturbation upon point mutation

The EPR spectrum of the Ne *c*-552 over-expressed in *E. coli* is shown in Figure 5E; it shows exactly the same *g*-resonances as those observed in the form isolated from *N. europaea*, with signals at g_{max} = 3.34, g_{mid} = 1.87 and g_{min} = 1.17, demonstrating that the expression system employed does not cause artifacts. In the mutant NeN64Δ (Figure 5F), where the asparagine residue is deleted, the resulting axial field is strongly suppressed and the three *g*-tensor resonances are clearly seen in the spectrum at g_{max} = 3.13(1), g_{mid} = 2.18(2) and g_{min} = 1.20 (2) characterized by $V = 1.36(2)\zeta$, $\Delta = 2.74(4)\xi$ and rhombic *vs* axial ratio $V/\Delta = 0.50$. The other Ne *c*-552 mutants, NeG50N/V65Δ and NeV65Δ, show very different EPR envelopes with g_{max} at 3.34(1) and 3.35(1) respectively (Figure 5G and 5H). The EPR spectra are depicted in Figure 5G and 5H, respectively. Both NeG50N/V65Δ and NeV65Δ show additional signals at $g_{max} \sim$ 3.1 and $g_{mid} \sim$ 2.2, revealing the coexistence of a rhombic component, with g_{mid} particularly enhanced in NeG50N/V65Δ. A similar effect has been observed previously in wild-type Ne *c*-552, where the rhombic species was found in a pH dependent equilibrium with the dominant HALS species.[25] Estimation of the g_{mid} values for the major axial species was furthermore complicated by the presence of anomalies around g = 2, due to an overlapping Cu^{2+} signal arising from impurities. Thus a rather large degree of uncertainty is associated with g_{mid} assignments. The g_{min} value is not detected in NeG50N/V65Δ, either by increasing or decreasing the microwave power or by further decreasing the sample temperature, while in

NeV65Δ a weak and broad signal is observed at 1.14 (Δν ~ 65 mT). The estimated g_{mid} component, together with its uncertainty range, was then used to evaluate the g_{min} term in NeG50N/V65Δ by applying eq. 3, assuming that all three *g* values are positive and similar to those characterizing the overexpressed Ne *c*-552. The calculated values for NeG50N/V65Δ converged to g_{mid} = 1.87 ± 0.10 and g_{min} = 1.15 ± 0.17. The crystal-field correlation for NeV65Δ gave V= 1.06(5)ξ, Δ = 4.30 ± 0.06ξ, and ratio V/Δ = 0.25, while for NeG50N/V65Δ it gave V = 1.08(6)ξ, Δ = 4.78 ± 1.70ξ and V/Δ = 0.23. The rhombic V factors are therefore almost identical in these two mutants and in Ne *c*-552, as the overall envelopes are very similar to each other. The Δ values for NeV65Δ, NeG50N/V65Δ and Ne *c*-552 also are in a comparable range. Taking all these results with caution, the mutation or deletion of residues 50 and 65 in the variants NeV65Δ and NeG50N/V65Δ did not alter the electronic properties of the heme core, while NeN64Δ experienced an almost complete conversion to a rhombic species.

From the solution NMR studies reported above, NeV65Δ and Ne *c*-552 show axial Met fluxionality as well as minor rhombic components in their EPR spectra, and it is reasonable to consider that these observations may be related. However, neither NeN64Δ nor NeG50N/V65Δ show Met fluxionality (See Table 1) even though the presence of minor rhombic species was clearly detected in their EPR spectra. Therefore no direct correlation exists between a fluxional methionine as observed by NMR at 274-300 K, which in principle should favor distribution of ligand-field terms associated with the heme core, and detection of minor rhombic signals, as observed in most of the large g_{max} and HALS EPR spectra recorded at cryogenic temperatures. A caveat is that detection of Met fluxionality by solution NMR may not be possible over the accessible temperature range.

The microwave power saturation behavior of Pa c-551 and Ne c-552 mutants

In more axial systems with large g_{max} values (HALS) and rhombic systems with small *g*-anisotropy, the EPR envelopes saturate evenly (across the resonance) under increasing microwave power. The HALS envelopes in particular have the tendency to saturate at higher microwave energy compared to “rhombic” resonances. This indicates a more efficient spin-lattice relaxation (T_1) associated with the heme core for HALS species. In order to gain further knowledge about such relaxation properties at low temperatures, the magnetic behavior of the cytochrome *c* mutants (PaN64V, PaN64Q, PaN50G/V65ins, NeN64Δ, NeV65Δ and NeG50N/V65Δ) was compared and analyzed with respect to their wild-type counterpart (Pa *c*-551 and Ne *c*-552) by using the Portis[62] and Castner[63] theory. The resulting EPR spectra are collected in Figure 6. Representative saturation trends are shown in Figure 7, and the numerical fitting values for all the cytochromes under study, obtained through eq. 4 (See Materials and Methods), are shown in Table 2. It should be noticed that eq. 4 cannot be rigorously applied to strain-broadened EPR lines. In addition, the g_{max} resonances have lower transition probability than the g_{mid} and g_{min} components; therefore the calculation of the saturation trends was performed only around the g_{max} components. This is even more pertinent here, because several of the observed EPR envelopes of the mutants show the presence of anomalies around g ~ 2 (Cu^{2+} impurities) and extremely broad g_{min} signals which were completely undetected in some cases. In the Pa *c*-551 mutant series the $P_{1/2}$ saturation tendencies are almost identical, ranging from 38.10 ± 2.30 mW for PaN64V up to 43.60 ± 3.93 mW for PaN64Q. The saturation values for the mutants are very close to that measured in the over expressed Pa c-551 ($P_{1/2}$ = 44.30 ± 2.86 mW). In all these cases, the g_{max} signal always exhibited a Gaussian line-shape (b ~ 1 and half-width ~18-20 mT), with no line-shape distortions upon increasing the applied microwave energy (Figure 6A-6C). In the Ne *c*-552 mutant series, all proteins are characterized by quite large $P_{1/2}$ saturation values, similar to those observed for the Pa *c*-551 variants. However, the $P_{1/2}$ of the less axial system, NeN64Δ (40.60 ± 2.12 mW), is notably smaller than that of the more axial NeV65Δ ($P_{1/2}$ = 54.50 ± 2.41 mW), but nearly identical to the value previously determined for the wild type Ne *c*-552 ($P_{1/2}$ = 42.80 ± 4.20 mW). In the mutant NeN64Δ the

g_{max} signal can be simulated by assuming a Gaussian line-shape with the absence of line-shape distortions even under high microwave energy. For the NeV65Δ mutant, however, the g_{max} resonance line is always asymmetric, showing no dissimilarity in the saturation trends for low-field peak and high-field shoulder (Figure 6E), in harmony with what was observed previously in the wild-type form of Ne *c*-552. Many cytochromes with bis-His axial iron coordination and featuring HALS signals display such pronounced behavior at g_{max}, with a so-called "sharp cut-off" of the peak on the low-magnetic field side.[27,30,31] This phenomenon was addressed in the literature by invoking the presence of multiple species[30] or *g*-strain effects, which are regarded as micro-heterogeneities in the protein conformation occurring upon freezing.[31] Nevertheless in cytochrome *f* (N-terminal amine and His as axial ligands for the iron), that features a HALS EPR signal as well, such "sharp cut-off" of the peak at g_{max} = 3.51 is not witnessed and it exhibits an approximately Gaussian line-shape.[64] Here, the NeG50N/V65Δ mutant (Figure 6G) reveals very peculiar differences compared to the other axial mutant NeV65Δ and to the wild-type form of Ne *c*-552. In NeG50N/V65Δ the g_{max} line features the presence of two different components which are characterized by very different saturation behaviors. At low microwave power (~ 2 mW at T = 10 K), the high-field shoulder (marked as g_1 at ~ 225 mT) is already difficult to detect, leaving only one dominant axial signal (g_{max}) that emerges upon further increase of the microwave energy. This resonance is well described by a Gaussian line-shape at high microwave power. Furthermore, the broadening and weakening of the g_{max} shoulder (g_1) mirrors the weakening trend of the signal at 304 mT (marked as g_2 in Figure 6G) and hence both resonances constitute the g_1 and g_2 components of a rhombic heme. For that reason, meaningful extraction of the $P_{1/2}$ value in NeG50N/V65Δ has not been achieved. Temperature dependence of the EPR signals followed the Curie law in all cases examined, consistent with isolated $S = 1/2$ spin systems, with the only exception of NeG50N/V65Δ, which showed deviations from linearity. The EPR signals were practically not observed over 30 K for any sample, over-expressed forms and mutants. In this respect, the observed trends for the mutants PaN64V and NeN64Δ, are shown in Figure 6D and Figure 6H respectively, as an example of the analogous temperature behaviors.

Correlation between EPR and NMR results

Comparison of the NMR and EPR results (Table 1 and Table 2 respectively) does not reveal any direct relationship between the presence of axial Met dynamics and observation of axial EPR spectra, nor between Met orientation (A, B) and *g*-tensor parameters; however a linear correlation is seen between the observed g_{max} values in this mutant series or their derived ligand-field anisotropy (V/Δ ratio) *versus* the averaged heme methyl chemical shift <δ> with a general form $g_{max} = f(<\delta>)$ or $V/\Delta = f(<\delta>)$, albeit with a fair amount of scatter, with R = 0.95 for $g_{max} f(<\delta>)$ and R = 0.97 for $V/\Delta\ f(<\delta>)$ (Figure 8A and Figure 8B respectively). This finding is reminiscent of the linear relationship observed between g_{max} (or $|g_{zz}|$) and V/Δ with A_{zz}, as determined from Mössbauer data.[27] The correlation shows that i) when the g_{max} signal increases, the average methyl chemical shift <δ> increases and ii) when the ligand field anisotropy V/Δ increases (from more axial to rhombic), the average methyl chemical shift <δ> decreases. The linear correlation holds fairly well when other experimental data (g_{max}, V/Δ and <δ>) available for similar cytochrome *c* proteins with His/Met axial ligation are included ($g_{max} f(<\delta>)$ with R = 0.93, $V/\Delta\ f(<\delta>)$ with R = 0.95) such as horse cytochrome *c*[61], *P. stutzeri c*-551,[47,65] *P. ZoBell c*-551,[47,66] *Rhodopseudomonas palustris c*-2,[67] and *Saccharomyces cerevisiae* iso-1 cyt *c*.[47,68] However, the linear trend observed does not accommodate *Bacillus pasteurii c*-553[69] and *Rhodospirillum rubrum c*-2[68], for which g_{max}, V/Δ and <δ> values fall well outside the linear region. This is even more pertinent when other combinations of axial heme ligands are considered, such as for example cytochrome *f* (N-terminal amine and His as axial iron ligands) with g_{max} at 3.51 and <δ> at 17.8 ppm,[64] cytochrome b_5 with g_{max} at 3.03 and <δ> at 11.1 ppm (bis His as axial ligands)[61] or MetMbCN with g_{max} at 3.45 and <δ> at 17.2 ppm (His and CN as axial ligands)[61] which values are much far away from the linear

trend reported in Figure 8 (see Supporting Information). Connection between ligand-field terms (V and/or Δ) and spectroscopic/magnetic parameters has been used extensively by several groups to predict axial ligand nature in low-spin ferriheme.[27,70,71] For example, in the original work of Gadsby and Thomson[26] it was shown by analyses of near-IR MCD transitions that a positive empirical linear correlation exists between the charge transfer transitions (E_{CT}) from the highest filled porphyrin orbitals, a_{1u} and a_{2u} (π), and the energy of the positive hole E_{yz} ($(\Delta/3+V/2)/\xi f E_{CT}$). Even though we consider in this work a limited number of Ne and Pa variants, these specific point mutations allow us to draw a similar linear correlation that links axial strain and averaged paramagnetic methyl shifts that stands irrespective of Met dynamics observed in NMR. However, this relation is clearly less general compared to that one introduced by Gadsby and Thomson and restricted only to cases that include closely related proteins and their mutants. Our findings can be summarized as follows by using illustrative examples: 1) PaN64V has an altered axial Met orientation (B, from A) and evidence of Met dynamics not observed in Pa *c*-551. This mutant also has a significantly more rhombic EPR spectrum (V/Δ = 0.55), lower g_{max}, (3.05, from 3.20) as well as lower <δ> (21.1, from 21.8) relative to Pa *c*-551. 2) The N64Q mutation of Pa *c*-551 causes the axial Met to display fluxionality, resulting in a large decrease in the spread of heme methyl shifts. However in PaN64Q the V/Δ ratio, g_{max} value and also <δ> show only minimal increases relative to Pa *c*-551. 3) In the mutant PaN50G/V65ins the V/Δ increases slightly (to 0.40), g_{max} decreases slightly (to 3.18) and <δ> is unchanged relative to Pa *c*-551. Consequently the Pa *c*-551 mutant series underlines the importance of one residue located in the second coordination sphere (here, Asn64) on preserving the axial strain of the system, but other factors may as well contribute. 4) The importance of residue Asn64 for maintaining the axial field is also encountered in the Ne *c*-552 mutants; in NeN64Δ the Met61 has orientation B as indicated by the heme methyl shift pattern while Ne *c*-552 displays Met ligand fluxionality. NeN64Δ exhibits a rhombic EPR spectrum with a lower g_{max} (3.13 from 3.34) as compared to Ne *c*-552, a larger V/Δ ratio (0.50 versus 0.24) and a lower <δ> (21.0, from 22.4). The observation of a relationship between <δ> with both g_{max} and V/Δ arises from the fact that the NMR paramagnetic shifts experienced by the porphyrin methyl groups are related to the spin density distribution (ρ_i^{π}) residing on the porphyrin core and thus to the magnetic anisotropy of the heme group itself.[52,54,55,61,72] From the knowledge of the χ tensor orientation and $\Delta\chi$ values, the magnetic susceptibility anisotropy, the contact shifts of the heme protons can be obtained.[61] However in the linear expressions $g_{max}f(<\delta>)$ and $V/\Delta\, f(<\delta>)$, the angular coefficient f should contain both electronic and structural parameters, which are difficult to quantify as explained below. The experimentally observed heme methyl shifts of horse cytochrome *c* (both order and magnitude), which at neutral pH has a rhombic EPR spectrum, were well predicted by Hückel calculations;[47] here the Met residue can be considered dominant in determining the orientation of the orbital hole. Such predictions are less accurate when very slight increments on the heme axial strain are present (as in the case of Pa *c*-551). In a very weak axial system, e.g. more axial compared to the rhombic cytochrome *c* at neutral pH, both Met and His axial ligands should contribute almost equally to determining the orientation (and energy) of the orbital hole. Indeed, this phenomenon may account for the small chemical shift range displayed by NeG50N/V65Δ. Furthermore, as suggested by Walker,[47] in such a case also other electronic contributions from excited states might be non-negligible, especially in the high temperature range.[61] This hypothesis is supported by recent DFT results obtained on a heme model of cytochrome *c*, which included the porphyrin ring, the methionine and the imidazole ring of the histidine group as axial ligand for the iron.[50] The spin density distributions ρ_i extracted for four different heme spin configurations upon considering the Fe atom in two distinct charged states, provided singlet and triplet states when zero charge resided on Fe, and doublet and quartet states when +3 charges were placed on Fe, showed that in the doublet state configuration, a positive spin density (1.11) is localized on the Fe atom, while negative spin density resides in the porphyrin ring (-0.69 in total) and very small negative spin density is located on both the sulfur atom of the Met group (-0.06) and the nitrogen coordinating atom of the imidazole moiety (-0.04).

However, the doublet (S=1/2) and the singlet (S=0) states have been found degenerate in energy with a low-lying excited quartet state (S= 3/2, 1.7 kcal/mol) and a higher energy excited triplet state (S=1, 17.5 kcal/mol). It thus appears that small electronic perturbations acting on each axial ligand (Met and/or His) that can modulate the net charge residing on the Fe atom can trigger substantial changes in the heme ligand-field anisotropy.

From the EPR findings, the more rhombic systems have relatively small <δ>; one possible cause for this effect might arise from the stronger interaction of the orbital hole with porphyrin orbitals that does not place the spin at the pyrroles, in particular, $a_{2u}(\pi)$. Indeed, when heme takes on a ruffled conformation, the predominant mode of distortion in cytochromes *c*,[73] interaction between the porphyrin $a_{2u}(\pi)$ and the iron d_{xy} becomes allowed, raising the energy of the d_{xy} orbital.[74,75] Such an effect would nicely explain the trends seen in this work. A heme group that is highly ruffled will have a smaller <δ> resulting from less unpaired electron density in the $3e_g(\pi_{x,y})$ orbitals. The heme ruffling will raise the energy of the d_{xy} orbital, decreasing Δ/ξ, and as a result promoting higher heme rhombicity. Thus it is possible that the engineered mutations impact here the heme conformation, similar to the findings observed for proximal heme pocket mutations in nitrophorins, which have been shown to alter heme ruffling.[76] Heme distortion can be evaluated directly through high-resolution crystal structures, which are available for some of the wild-type proteins presented in this work. Therefore the out-of-plane distortion for the heme macrocycle was measured in these proteins, using Shelnutt's Normal-coordinate Structural Decomposition program.[77] Among the proteins analyzed in this work for which structures are available, it is notable that Pa *c*-551 has a more planar heme (0.49 Å displacement), higher g_{max}, higher <δ> and smaller V/Δ as compared to the horse cytochrome *c* that exhibits a higher level of heme distortion (1.05 Å displacement), smaller g_{max}, smaller <δ>, larger V/Δ and a rhombic EPR spectrum. However, if we include in this series again the case of *Bacillus pasteurii c*-553 for which a high resolution (0.97 Å) X-ray structure is available,[43] such correlation between heme distortion and trend in g_{max} ,<δ> and V/Δ parameters stands qualitatively but does not fit within the linear trend seen in Figure 8. The same is true for *Rhodopseudomonas palustris* c_2. Because the structure of *B. pasteurii c*-553 shows a very planar heme group and furthermore in *R. palustris* c_2 a rather planar heme is present as well (1.70 Å resolution),[78] in the relations $g_{max}f(<\delta>)$ or V/Δ $f(<\delta>)$ the angular coefficient *f* contains certainly not only structural factors. One of the factors that might play a role here is the different redox potential characterizing these proteins. The $E^{0\prime}$ values of Class I cytochrome *c* vary from + 0.2 to + 0.35 Volt (versus NHE), where a significant contribution to their high potential is proposed to arise from the π-electron acceptor character of the sulphur atom of the methionine axial ligand that stabilizes the Fe^{2+} reduced state.[2] The Ne *c*-552 (+ 0.250 V),[5] Pa *c*-551 (+ 0.291 V),[11] cytochrome *c* from horse heart (+ 0.260 V),[2] *S. cerevisiae* (Yeast) iso-1 (+ 0.290 V)[79], *ZoBell c*-551 (+ 0.250 V)[80], *R. rubrum* c_2 (~ 0.310 V)[81] share a very similar $E^{0\prime}$ potential, while *B. pasteurii c*-553 exhibits a much lower $E^{0\prime}$ (+ 0.047 V)[69] and *R. palustris* c_2 has a larger $E^{0\prime}$ value (+ 0.350 V and/or + 0.365 V depending on conditions).[78,82] Several factors such as coordinative effects of the heme-ligands, hydrophobicity of the heme environment, differences in dynamics and solvation properties between the Fe^{3+}/Fe^{2+} redox states, all contribute to determine the redox value of the protein.[83] Nevertheless, $E^{0\prime}$ is also linked to the HOMO/Lowest Unoccupied Molecular Orbital (LUMO) gap and thus to the energy distribution of the frontier orbitals.[84] In this context, we finally speculate that the possible basis for the observed variation in <δ> which mirrors variations in V/Δ is that a lower <δ> should reflect a larger unpaired electron spin delocalization to the axial ligands (i.e., less unpaired electron density on the heme as a whole). Greater spin delocalization to the axial groups (Met and/or His) would correlate with stronger iron-ligand bonds, which is associated with greater ligand-field strength and thus a more rhombic configuration, in agreement with our observed correlations. However, DFT calculations on cytochrome *c* model[50] clearly showed that the spin density on the axial ligands is quite small, thus the expected difference in the spin distribution allocated on the axial ligands under action

of different degrees of axial strain it is likely to be too small to be predicted with accuracy by DFT. Additional experiments probing directly the bond strengths of the Fe-His and the Fe-Met through XAS at Fe and S-edge and EXAFS on this series of proteins would be needed to ultimately test this hypothesis.

We find here that when Met and His act as axial ligands, no clear-cut difference exists between the large g_{max} and the "small *g*-anisotropy" cases, but even slight electronic perturbations of the methionine ligand, as shown in this work, are enough to trigger the ligand field to change from (weakly) axial to rhombic. Even though we did not succeed in the reverse process, namely strengthening the axial field starting from a weaker one like in Pa *c*-551, the availability of cytochrome *c* mutants having finely tuned ligand-field anisotropy will ultimately allow systematic, controlled studies of the influence of heme pocket structure and electronic structure on the heme electron-transfer reactivity. The detailed knowledge of EPR (*g* anisotropy, ligand-field terms) and NMR (<δ>, Met orientation) data on similar heme proteins with His-Met axial iron ligation would ultimately add valuable information for further testing of the hypotheses reported here. For example, it would be interesting to compare the <δ> from the Ne diheme peroxidase which has a g_{max} at 3.38[19] as it has the axial Met ε-CH_3 directed towards pyrrole III (1BGY.pdb), which is different from the orientations A or B. Thus in conclusion with Met-His axial iron coordination no clear-cut difference exists between the "large g_{max}" and "normal" (lower g_{max}) cases, such as is noted for bis-His axial coordination with perpendicular His-planes. The lack of correlation between EPR data and heme axial Met orientation or dynamics reinforces the importance of NMR spectroscopy for providing detailed and accurate information about the nature of heme axial ligation for hemes, in particular for those with His/Met axial ligation.

Supplementary Material

Refer to Web version on PubMed Central for supplementary material.

ACKNOWLEDGMENT

This work was supported by the Research Council of Norway Grant 177661/V30 (K.K.A.) and Grant 157855 (E.H., and K.K.A.), and from The National Institute of Health (NIH) of the United States of America Grant GM63170 (R.K., A.A.E. and K.L.B.) We thank Dr. Hans Petter Hersleth (University of Oslo) for the protein structural drawings depicted in Figure 1.

Glossary

Abbreviations:

NMR
: nuclear magnetic resonance

NOESY
: 2-dimensional Nuclear Overhauser Enhancement Spectroscopy

TOCSY
: Total Correlation Spectroscopy

EPR
: Electron Paramagnetic Resonance

Pa *c*-551
: *Pseudomonas aeruginosa* cytochrome *c*-551

Ne *c*-552

Nitrosomonas europaea cytochrome *c*-552

PDB

Protein Data Bank

REFERENCES

(1). Pettigrew, GW.; Moore, GR. Cytochromes c. Biological Aspects. Springer Verlag, Berlin - Heidelberg; New York: 1987.

(2). Moore, GR.; Pettigrew, GW. Cytochromes c. Evolutionary, Structural, and Physicochemical Aspects. Springer Verlag, Berlin - Heidelberg; New York: 1990.

(3). Ambler RP. Biochim. Biophys. Acta 1991;1058:42–47. [PubMed: 1646017]

(4). Michel LV, Ye T, Bowman SEJ, Levin BD, Hahn MA, Russell BS, Elliott SJ, Bren KL. Biochemistry 2007;46:11753–11760. [PubMed: 17900177]

(5). Timkovich R, Bergmann D, Arciero DM, Hooper AB. Biophys. J 1998;75:1964–1972. [PubMed: 9746537]

(6). Muegge I, Qi XP, Wand AJ, Chu ZT, Warshel A. J. Phys. Chem. B 1997;101:825–836.

(7). Peisach J, Blumberg WE, Adler A. Ann. N. Y. Acad. Sci 1973;206:310–327. [PubMed: 4356182]

(8). Blumberg, WE. Magnetic resonance in biological systems. Ehrenberg, A.; Malmström, BG.; Vänngård, T., editors. Pergamon; 1967. p. 119-133.

(9). Neese F. Curr. Op. Chem. Biol 2003;7:125–135.

(10. Bren KL, Kellogg JA, Kaur R, Wen X. Inorg. Chem 2004;43:7934–7944. [PubMed: 15578827]

(11). Terui N, Tachiiri N, Matsuo H, Hasegawa J, Uchiyama S, Kobayashi Y, Igarashi Y, Sambongi Y, Yamamoto Y. J. Am. Chem. Soc 2003;125:13650–13651. [PubMed: 14599189]

(12). Horio T, Higashi T, Sasagawa T, Kusai K, Nakai M, Okunuki K. Biochem. J 1960;77:194–201. [PubMed: 13715846]

(13). Silvestrini MC, Tordi MG, Antonini E, Brunori M. Biochem. J 1982;203:445–451. [PubMed: 6288000]

(14). Cutruzzolà F, Ciabatti I, Rolli G, Falcinelli S, Arese M, Ranghino G, Anselmino A, Zennaro E, Silvestrini MC. Biochem. J 1997;322:35–42. [PubMed: 9078240]

(15). Cutruzzolà, F.; Arese, M.; Brunori, M. Handbook of Metalloproteins. Wiley; Chichester: 2001. Cytochrome c-551.

(16). Matsuura Y, Takano T, Dickerson RE. J. Mol. Biol 1982;156:389–409. [PubMed: 6283101]

(17). Detlefsen DJ, Thanabal V, Pecoraro VL, Wagner G. Biochemistry 1991;30:9040–9046. [PubMed: 1654086]

(18). Yamazaki T, Fukumori Y, Yamanaka T. J. Biochem 1988;103:499–503. [PubMed: 2839468]

(19). Arciero DM, Hooper AB. J. Biol. Chem 1994;269:11878–11886. [PubMed: 8163487]

(20). Yamanaka T, Shinra M. J. Biochem. (Tokyo) 1974;75:1265–1273. [PubMed: 4372235]

(21). Wen X, Bren KL. Inorg. Chem 2005;44:8587–8593. [PubMed: 16271000]

(22). Timkovich R, Cai ML, Zhang BL, Arciero DM, Hooper AB. Eur. J. Biochem 1994;226:159–168. [PubMed: 7957244]

(23). Russell BS, Zhong L, Bigotti MG, Cutruzzolá F, Bren KL. J. Biol. Inorg. Chem 2003;8:156–166. [PubMed: 12459911]

(24). Arciero DM, Peng Q, Peterson J, Hooper AB. FEBS Lett 1994;342:217–220. [PubMed: 8143881]

(25). Zoppellaro G, Teschner T, Harbitz E, Schünemann V, Karlsen S, Arciero DM, Ciurli S, Trautwein AX, Hooper AB, Andersson KK. Chem. Phys. Chem 2006;7:1258–1267. [PubMed: 16688708]

(26). Gadsby PMA, Thomson AJ. J. Am. Chem. Soc 1990;112:5003–5011.

(27). Walker FA. Coord. Chem. Rev 1999;185-186:471–534.

(28). Palmer, G. Physical Methods in Bioinorganic Chemistry, Spectroscopy and Magnetism. Lawrence, Que, Jr., editor. University Science Books; Sausalito California: 2000. p. 121-185.

(29). Paul MA, Gadsby PMA, Thomson AJ. FEBS Lett 1986;197:253–257.

(30). De Vries S, Albracht SPJ. Biochim. Biophys. Acta 1979;546:334–340. [PubMed: 221015]

(31). Salerno JC. J. Biol. Chem 1984;259:2331–2336. [PubMed: 6321467]
(32). Walker FA, Huynh BH, Scheidt WR, Osvath SR. J. Am. Chem. Soc 1986;108:5288–5297.
(33). Migita CT, Migita K. Biochim. Biophys. Acta 1983;743:290–298. [PubMed: 6297601]
(34). Griffith JS. Nature 1957;180:30–31. [PubMed: 13451631]
(35). Taylor CPS. Biochim. Biophys. Acta 1977;491:137–149. [PubMed: 191085]
(36). Griffith JS. Mol. Phys 1971;21:135–139.
(37). Alonso PJ, Martínez JI, García-Rubio I. Coord. Chem. Rev 2007;251:12–24.
(38). Walker FA. Chem. Rev 2004;104:589–615. [PubMed: 14871136]
(39). Teschner T, Yatsunyk L, Schunemann V, Paulsen H, Winkler H, Hu C, Robert Scheidt W, Walker FA, Trautwein AX. J. Am. Chem. Soc 2006;128:1378–1389.
(40). Ikenue T, Ohgo Y, Saitoh T, Yamaguchi T, Nakamura M. Inorg. Chem 2001;40:3423–3434. [PubMed: 11421688]
(41). Orme-Johnson RN, Hansen RE, Beinert H. J. Biol. Chem 1974;249:1928–1939. [PubMed: 4361833]
(42). Cheesman MR, Little PJ, Berks BC. Biochemistry 2001;40:10562–10569. [PubMed: 11523998]
(43). Benini S, González A, Rypniewski WR, Wilson KS, Van Beeumen J, Ciurli S. Biochemistry 2000;39:13115–13126. [PubMed: 11052663]
(44). Hanson GR, Gates KE, Noble JC, Griffin M, Mitchell A, Benson S. J. Inorg. Biochem 2004;98:903–916. [PubMed: 15134936]
(45). Walker FA, Nasri H, Turowska-Tyrk I, Moanrao K, Watson CT, Shokhirev NV, Debrunner PG, Scheidt WR. J. Am. Chem. Soc 1996;118:12109–12118.
(46). Senn H, Wüthrich K. Q. Rev. Biophys 1985;18:111–134. [PubMed: 3006116]
(47). Shokhirev NV, Walker FA. J. Biol. Inorg. Chem 1998;3:581–594.
(48). Griffith JS. Nature 1957;180:30–31. [PubMed: 13451631]
(49). Sato F, Yoshihiro T, Era M, Kashiwagi H. Chem. Phys. Lett 2001;341:645–651.
(50). Kumar A, Mishra PC, Verma CS, Renugopalakrishnan V. Int. J. Q. Chem 2005;102:1002–1009.
(51). Longuet-Higgins RC, Rector CW, Platt JR. J. Chem. Phys 1950;18:1174–1181.
(52). Shulman RG, Glarum SH, Karplus M. J. Mol. Biol 1971;57:93–115. [PubMed: 5089700]
(53). Lee K-B, La Mar GN, Mansfield KE, Smith KM, Pochapsky TC, Sligar SG. Biochim. Biophys. Acta 1993;1202:189–199. [PubMed: 8399380]
(54). Banci L, Bertini I, Luchinat C, Pierattelli R, Shokhirev NV, Walker FA. J. Am. Chem. Soc 1998;120:8472–8479.
(55). Turner DL. Eur. J. Biochem 1995;227:829–837. [PubMed: 7867644]
(56). Zhong L, Wen X, Rabinowitz TM, Russell BS, Karan EF, Bren KL. Proc. Natl. Acad. Sci. U.S.A 2004;101:8637–8642. [PubMed: 15161973]
(57). Wen X, Bren KL. Inorg. Chem 2005;44:8587–8593. [PubMed: 16271000]
(58). Shokhirev NV, Walker FA. J. Am. Chem. Soc 1998;120:981–990.
(59). Low DW, Gray HB, Duus JØ. J. Am. Chem. Soc 1997;119:1–5.
(60). Burns PD, La Mar GN. J. Biol. Chem 1981;256:4934–4939. [PubMed: 6262309]
(61). Bertini I, Luchinat C, Parigi G. Eur. J. Inorg. Chem 2000:2473–2480.
(62). Portis AM. Phys. Rev 1953;91:1071–1078.
(63). Castner TJ Jr. Phys. Rev 1959;115:1506–1515.
(64). Rigby SEJ, Moore GR, Gray JC, Gadsby PMA, George SJ, Thomson AJ. Biochem. J 1988;256:571–577. [PubMed: 3223931]
(65). H. VanWonderen J, Knight C, Oganesyan VS, George SJ, Zumft WG, Cheesman MR. J. Biol. Chem 2007;282:28207–28215. [PubMed: 17623666]
(66). Cheesman MR, Ferguson SJ, Moir JWB, Richardson DJ, Zumft WG, Thomson AJ. Biochemistry 1997;36:16267–16276. [PubMed: 9405061]
(67). Bertini I, Luchinat C, Macinai R, Martinuzzi S, Pierattelli R, Viezzoli MS. Inorg. Chim. Acta 1998;269:125–134.
(68). Brautigan DL, Feinberg BA, Hoffman BM, Margoliash E, Peisach J, Blumberg WE. J. Biol. Chem 1977;252:574–582. [PubMed: 13072]

(69). Benini S, Borsari M, Ciurli S, Dikiy A, Lamborghini M. J. Biol. Inorg. Chem 1998;3:371–382.

(70). Blumberg WE, Peisach J. Adv. Chem. Ser 1971;100:271–291.

(71). Mims WB, Peisach J. J. Chem. Phys 1976;64:1074–1091.

(72). Turner DL. Eur. J. Biochem 1993;211:563–568. [PubMed: 8382155]

(73). Jentzen W, Ma JG, Shelnutt JA. Biophys. J 1998;74:753–763. [PubMed: 9533688]

(74). Rivera M, Caignan GA. Anal. Bioanal. Chem 2004;378:1464–1483. [PubMed: 15214408]

(75). Ohgo Y, Hoshino A, Okamura T, Uekusa H, Hashizume D, Ikezaki A, Nakamura M. Inorg. Chem 2007;46:8193–8207. [PubMed: 17725347]

(76). Shokhireva TK, Berry RE, Uno E, Balfour CA, Zhang HJ, Walker FA. Proc. Natl. Acad. Sci. U.S.A 2003;100:3778–3783. [PubMed: 12642672]

(77). Shelnutt, JA. Normal-Coordinate Structural Decomposition (NSD) Program for emeproteins. http://jasheln.unm.edu/jasheln/content/nsd/nsd_welcome.htm

(78). Geremia S, Garau G, Vaccari L, Sgarra R, Viezzoli MS, Calligaris M, Randaccio L. Protein Sci 2002;11:6–17. [PubMed: 11742117]

(79). Berguis AM, Guillemette JG, Smith M, Brayer GD. J. Mol. Biol 1994;235:1326–1341. [PubMed: 8308895]

(80). Liang Q, Miller GT, Beeghley CA, Graf CB, Timkovich R. Biophys. J 2007;93:1700–1706. [PubMed: 17496029]

(81). Salemme FR. Ann. Rev. Biochem 1977;46:299–329. [PubMed: 197877]

(82). Battistuzzi G, Borsari M, Ferretti S, Sola M, Soliani E. E. J. Biochem 1995;232:206–213.

(83). Battistuzzi G, Borsari M, Sola M. Antioxid. Redox Signal 2001;3:279–291. [PubMed: 11396482]

(84). Rubensson HE, Jensen HJA. Chem. Phys. Lett 2006;432:591–594.

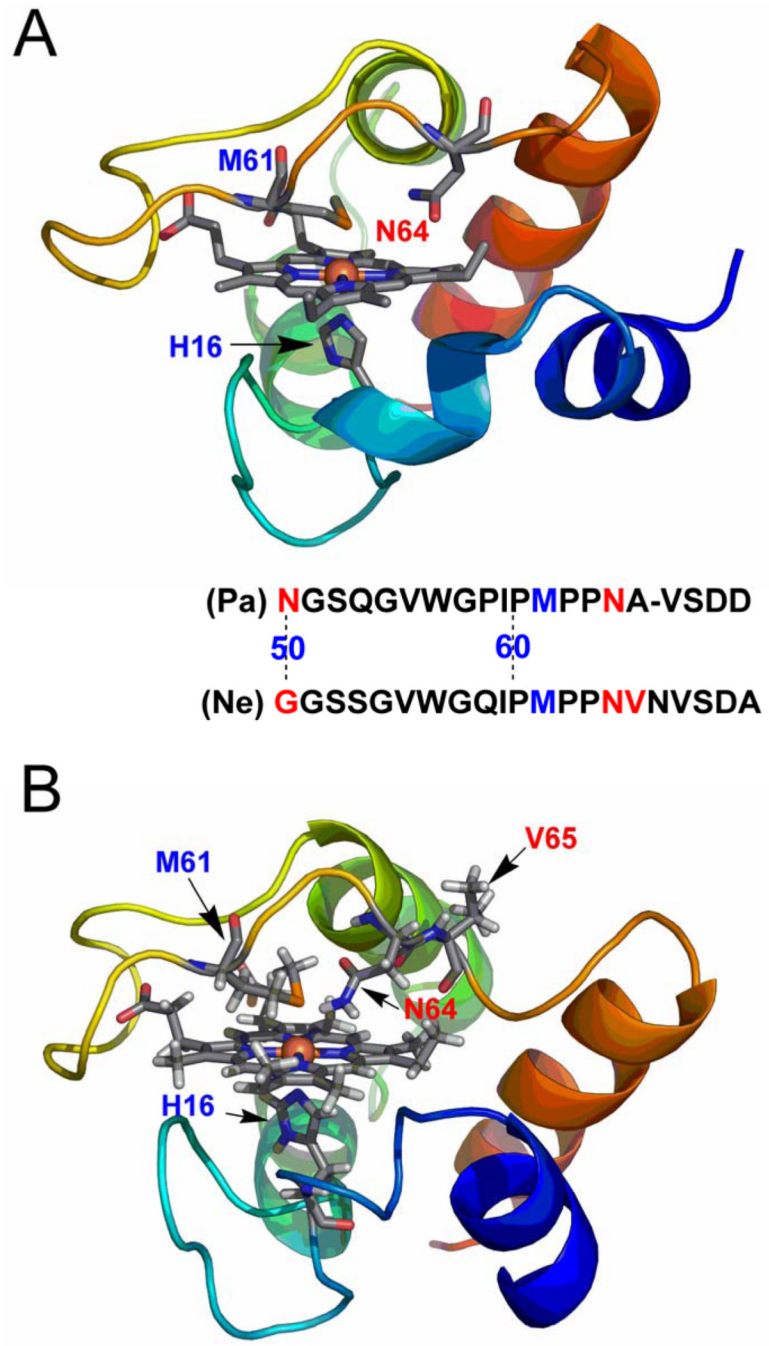

FIGURE 1.

Structure of (A) Pa *c*-551 (PDB code 351c) and (B) Ne *c*-552 (PDB code 1A56). The point mutations on selected residues are highlighted in the amino acid sequence in red while the Met axial ligand is highlighted in blue. Molecular drawings were made with the programme PyMOL, DeLano Scientific San Carlos, CA.

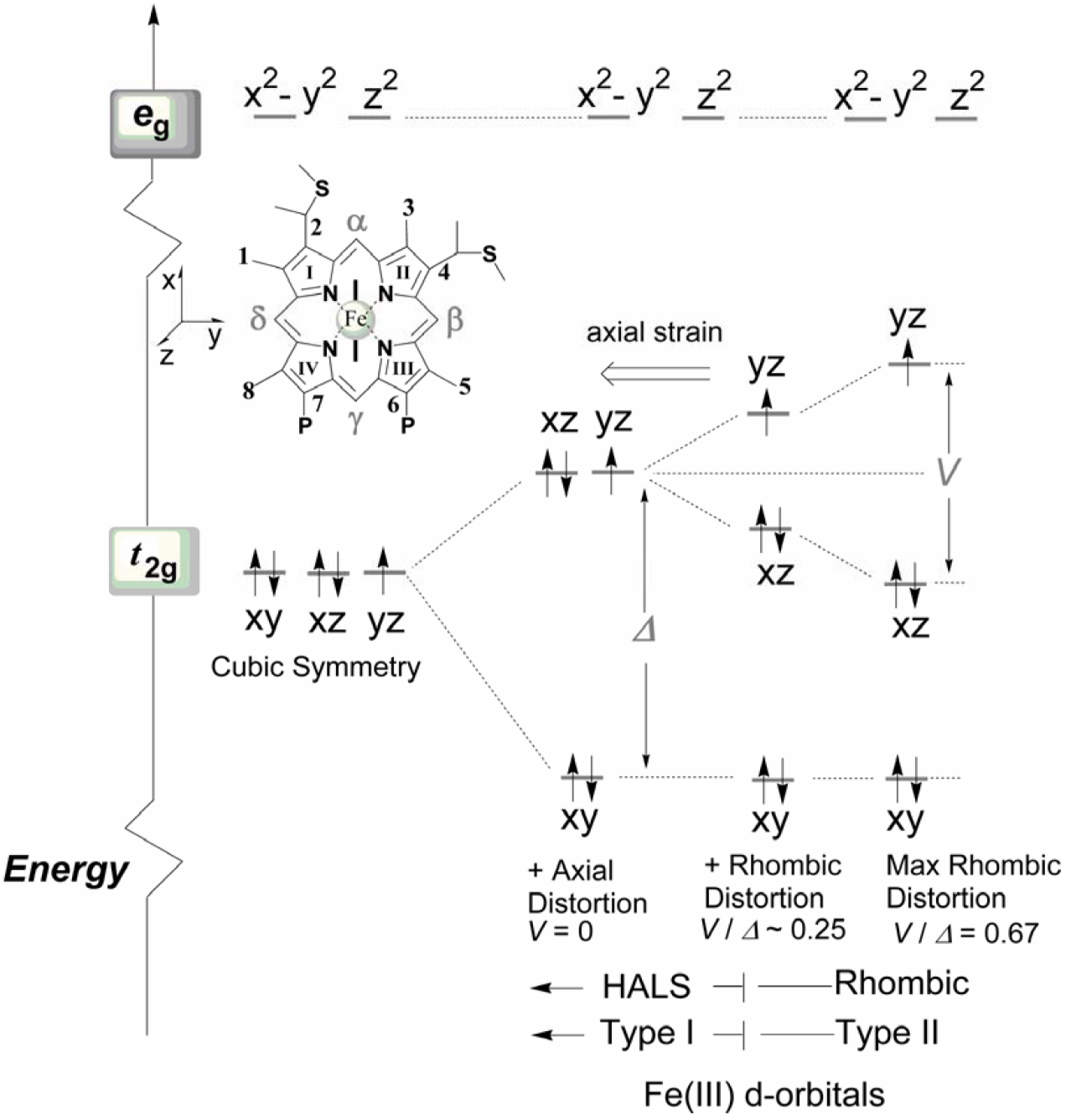

FIGURE 2.

Energy diagram of the d-orbitals level for low-spin ferric ion in with $(d_{xy})^2(d_{xz})^2(d_{yz})^1$ orbital occupancy. Note that the iron e_g orbitals are occupied when high spin and intermediate (e.g. S = 3/2) spin states are present in the system. The position of the axial histidine is shown in the sketch by a solid black line (—) in the porphyrin core oriented along the α-γ meso axis. The methionine residue is not depicted for clarity.

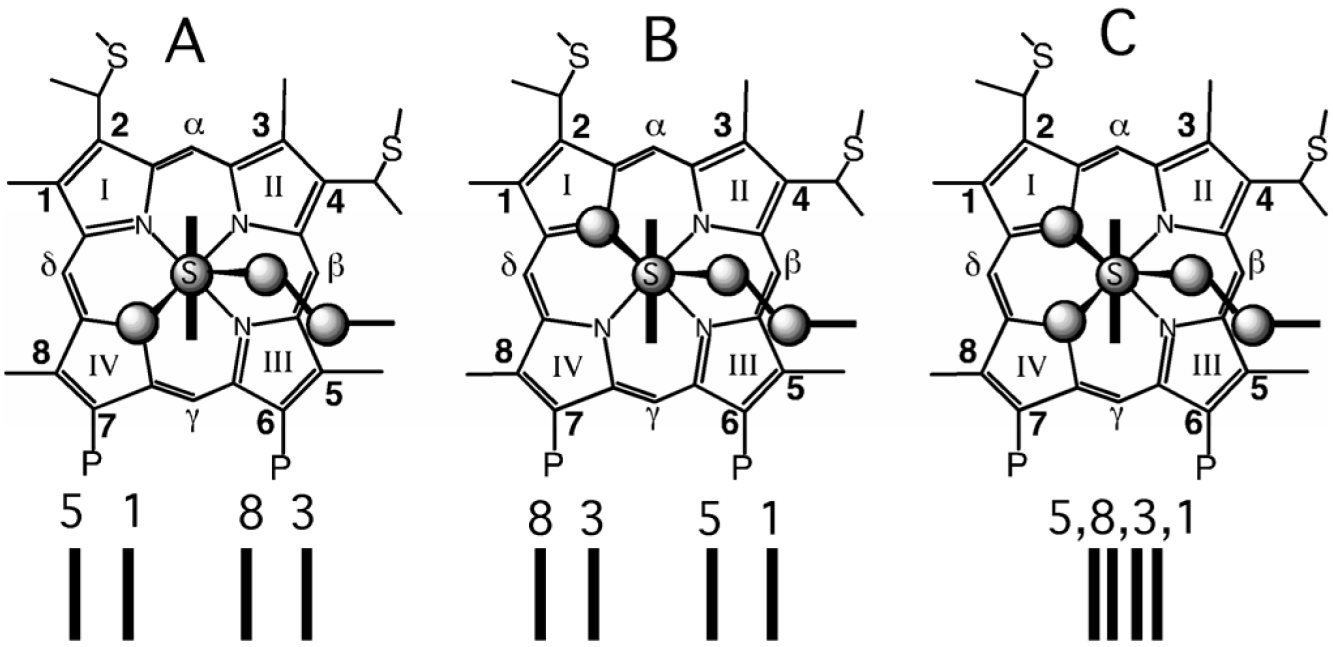

FIGURE 3.

Illustration of heme axial Met orientations and corresponding heme methyl ^{1}H NMR chemical shift patterns observed in cytochromes *c*. The Met side chain is shown in ball-and-stick format, and the plane of the axial His is shown as capped sticks. (A) Met orientation observed in PA resulting in a 5183 heme methyl shift pattern. (B) Met orientation in mitochondrial cyts *c*, resulting in a 8351 pattern. (C) Illustration of Met fluxionality with the Met sampling the conformations shown in (A) and (B). Ne *c*-552 shows such a compressed heme methyl shift pattern as a result of this phenomenon. Other shift patterns also are possible in case (C) and will depend on the conformations sampled by the Met and the chemical shifts in those conformations.

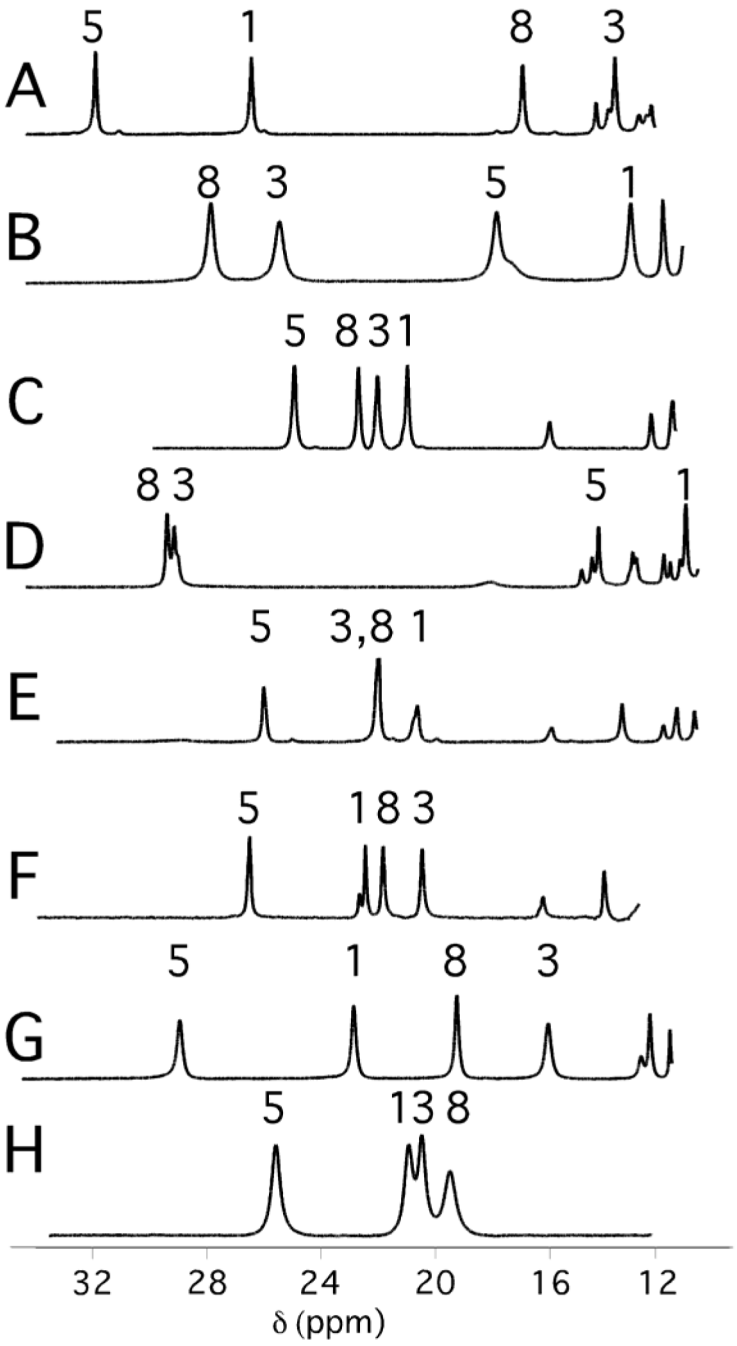

FIGURE 4.

Downfield region of ^{1}H NMR (500-MHz) spectra of (A) Pa *c*-551 (B) PaN64V (C) Ne *c*-552 (D) NeN64Δ (E) NeV65Δ (F) NeG50N/V65Δ(G) PaN50G/V65ins, (H) PaN64Q (from ref. [21]). Samples were 2-3 mM protein in 50 mM sodium phosphate buffer, pH 7.0, with 5× molar excess of $K_3[Fe(CN)_6]$, T = 299 K.

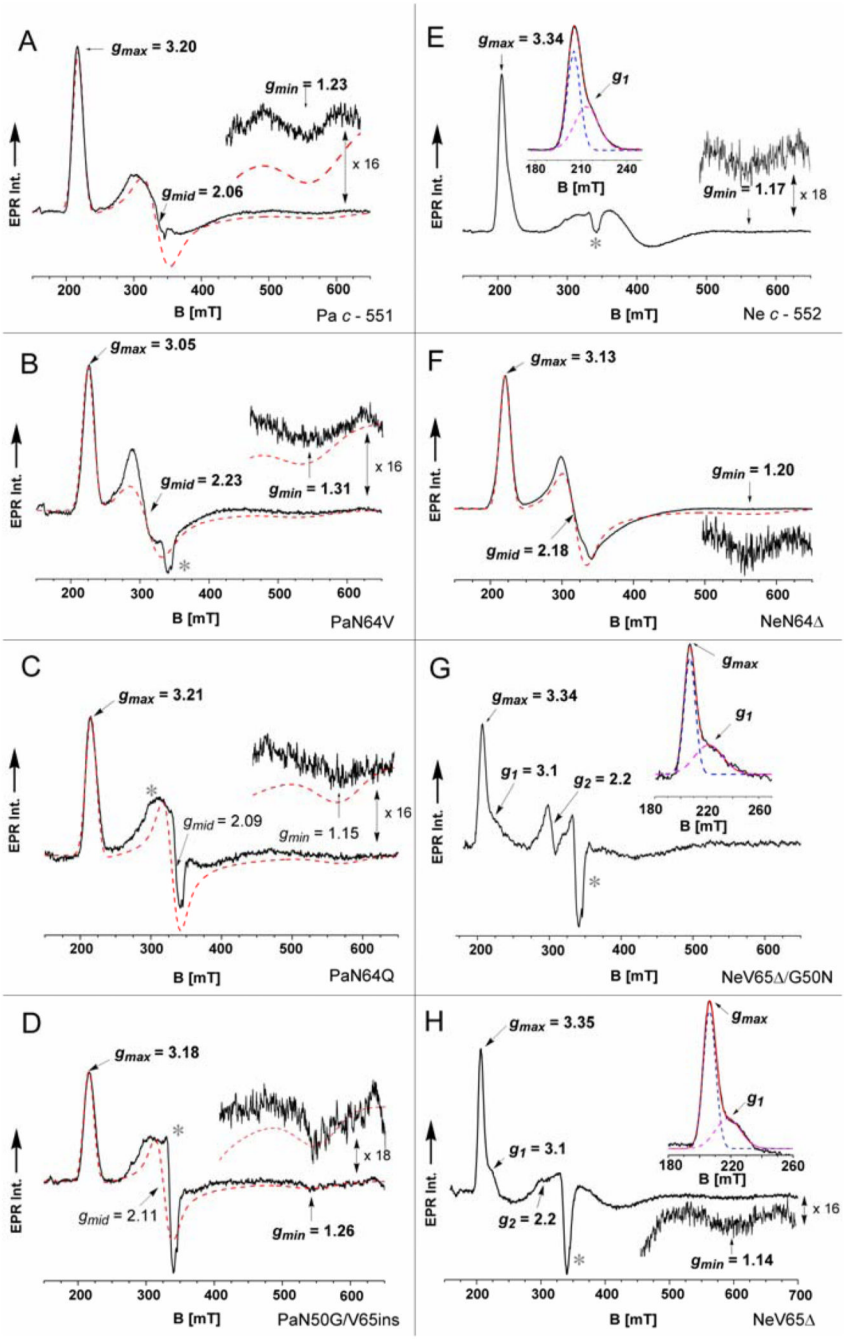

FIGURE 5.

The EPR spectra of (A) Pa *c*-551 (280 μM) (B) PaN64V (250 μM), (C) PaN64Q (220 μM), (D) PaN50G/V65ins (220 μM), (E) Ne *c*-552 cloned (310 μM), (F) NeN64Δ (260 μM), (G) NeG50N/V65Δ (210 μM), and (H) NeV65Δ (230 μM) in HEPES Buffer (50 mM, pH 7.5) recorded at 10.0 ± 0.5 K. In the EPR spectra the dashed lines represent simulated EPR envelopes. The asterisk (*) indicates the Cu^{2+} signal (g ~2) resulting from an impurity. The g factors in bold letters were observed experimentally, the others deduced by both spectra simulation and application of the g-tensor normalization conditions. The EPR spectra were acquired in the perpendicular mode by using the following experimental conditions: 9.662(8)

GHz, microwave power 1.0 mW excluding (G) recorded at 0.8 mW, modulation amplitude 0.75 mT, modulation frequency 100 KHz, 55 dB gain, sweep time 168 sec, time constant 82.92 msec; 4-6 scans were accumulated and averaged. The insets show magnification of the g_{max} and/or g_{min} resonances.

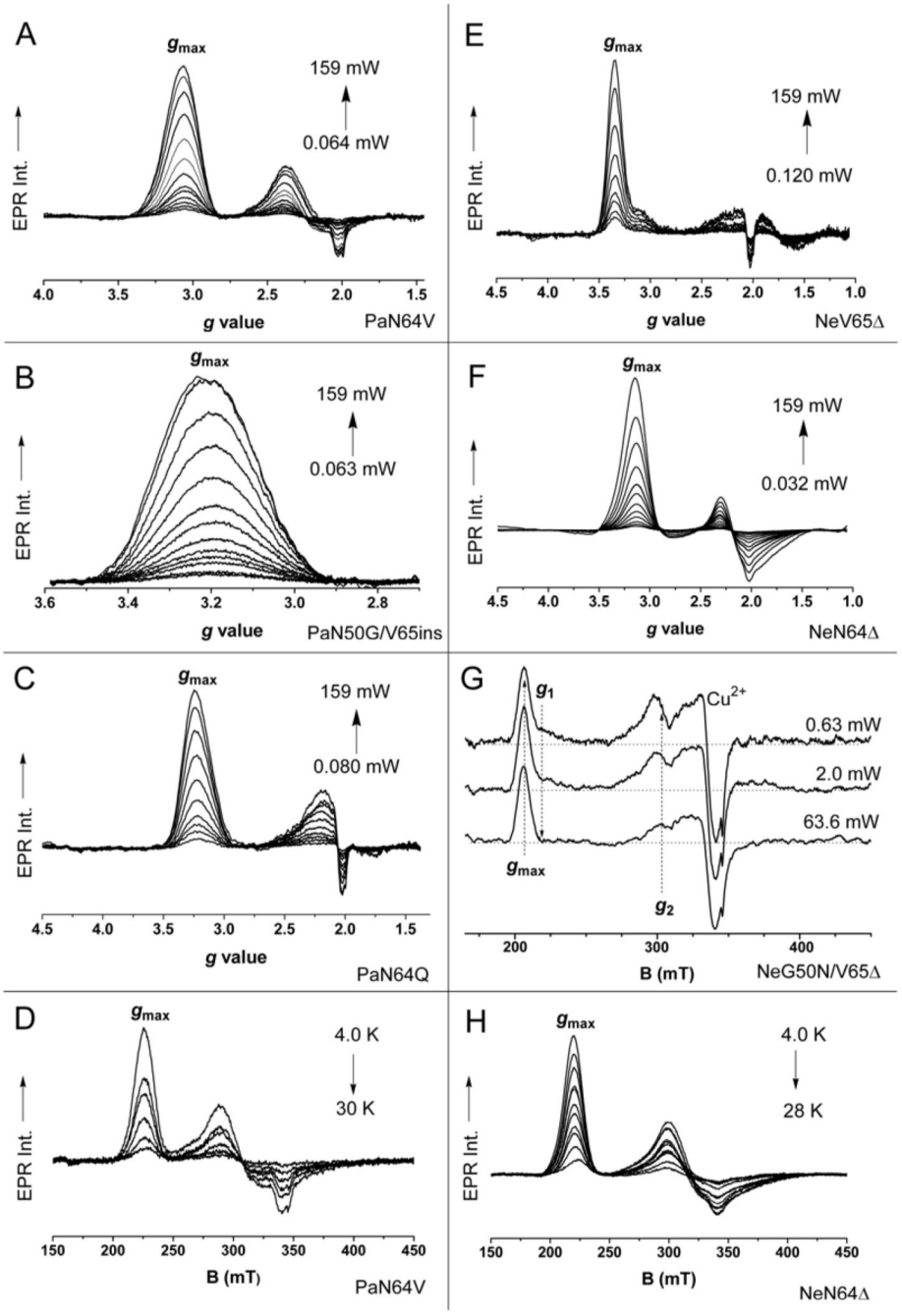

FIGURE 6.

The EPR spectra of (A) PaN64V, (B) PaN50G/V65ins, (C) PaN64Q, (E) NeV65Δ, (F) NeN64Δ and (G) NeG50N/V65Δ recorded under increasing microwave power at T = 10.0 ± 0.5 K. The temperature dependence is shown for EPR spectra of (D) PaN64V and (H) NeN64Δ. The EPR spectra were acquired in the perpendicular mode by using the following experimental conditions: 9.662(6) GHz, in (D) and (H) the microwave powers were kept constant at 0.32 mW, modulation amplitude 0.75 mT, modulation frequency 100 KHz, 55 dB gain, sweep time 83-168 sec, time constant 82.92 msec; 4 scans were accumulated and averaged.

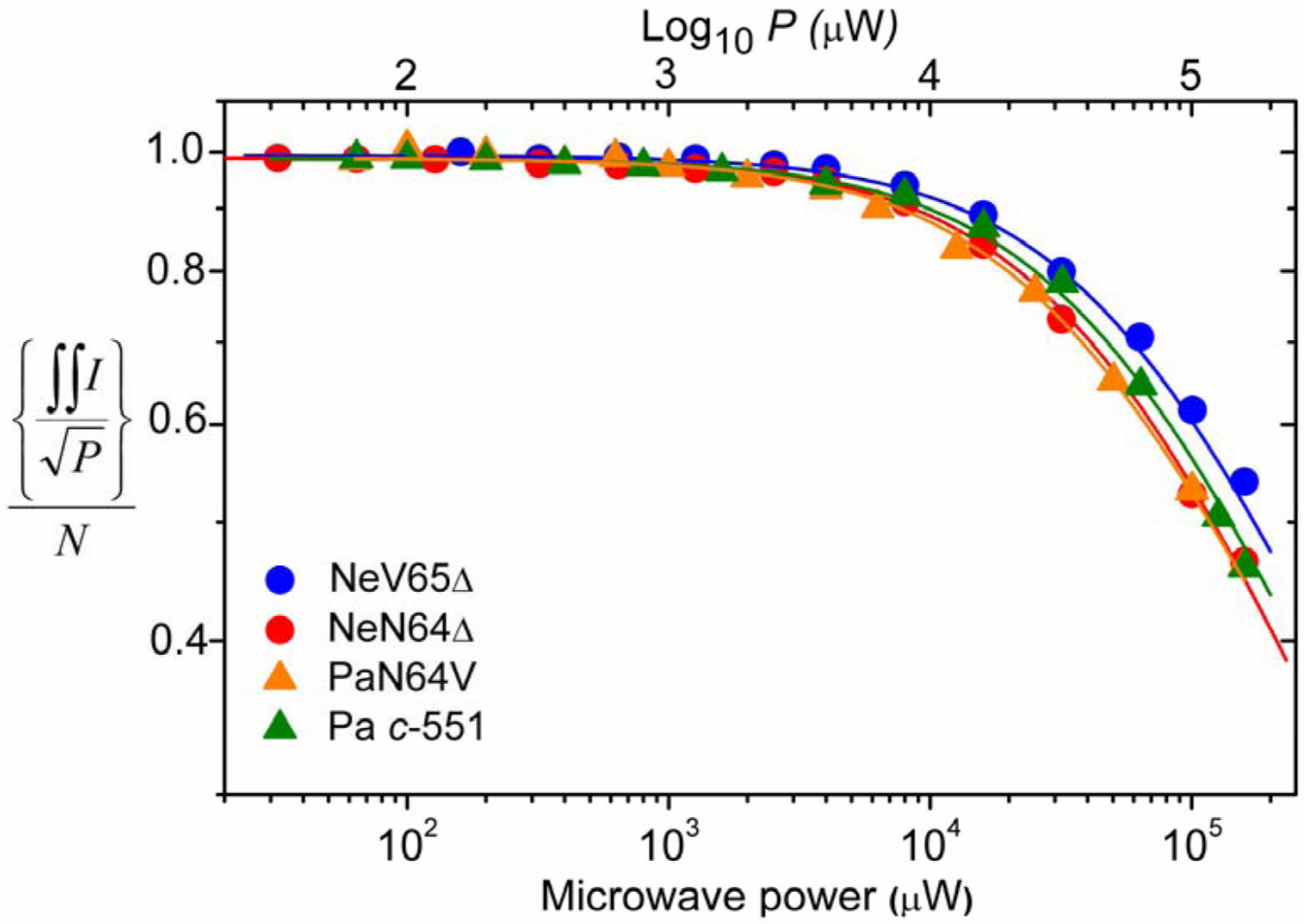

FIGURE 7.

Microwave power saturation trends of Pa c-551 (green triangle), PaN64V (orange triangle), NeN64Δ (red circle), and NeV65Δ (blue circle) performed by following the g_{max} signal. $\iint I$ represents the double integrated EPR signal intensity, P the applied microwave power and N the normalization constant. The correspondent simulations of the experimental data (triangles and circles) are shown by solid lines.

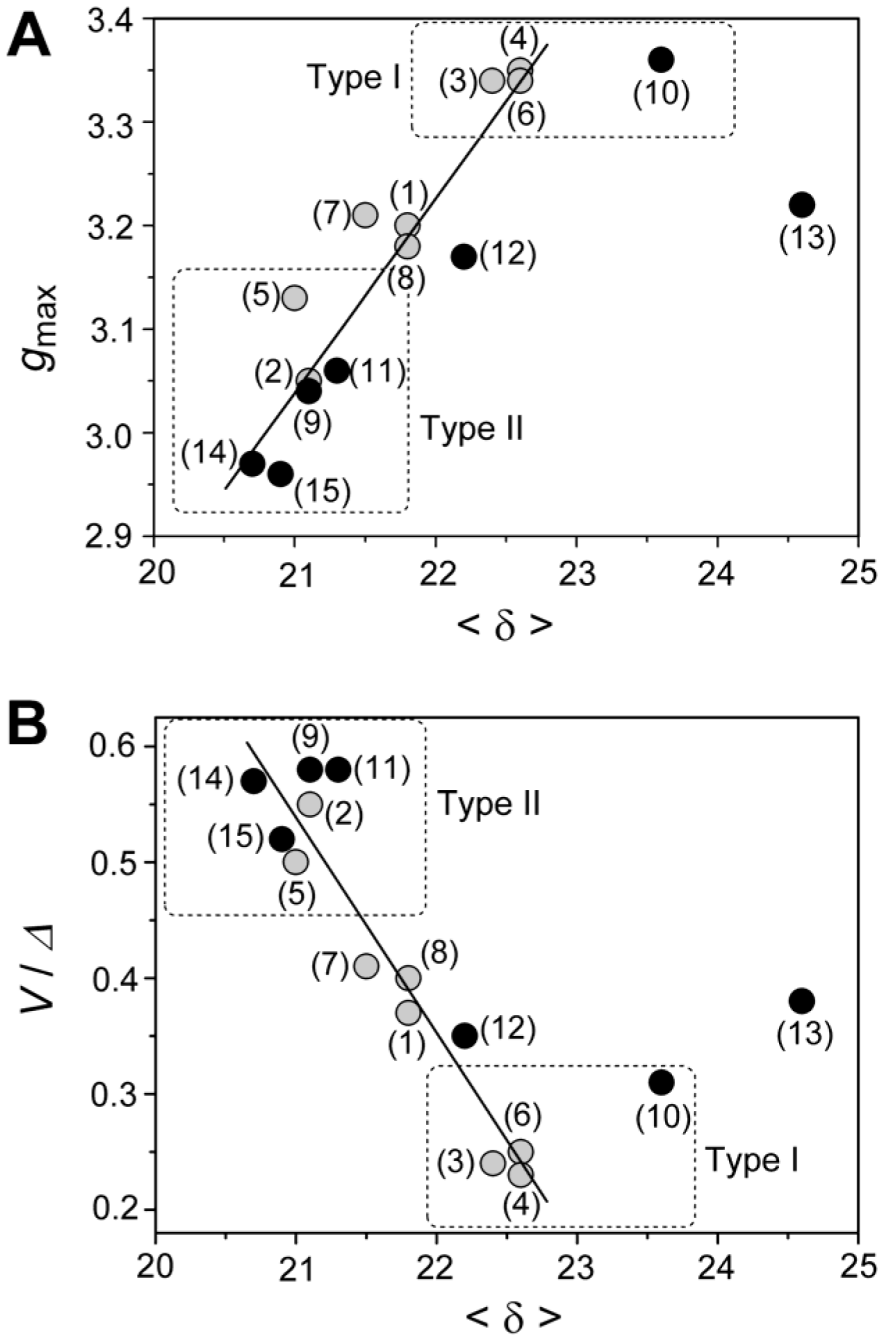

FIGURE 8.

Correlation between g_{max} values (A) or ligand-field anisotropy (V/Δ ratio) (B) *versus* the average heme methyl chemical shift <δ> in the over-expressed Ne *c*-552 and Pa *c*-551 proteins and their related mutants (grey circles, ●), together with different cytochrome *c* variants (black circles, ●). The cytochrome numbering scheme used (1-15) corresponds to that employed in both Table 1 and Table 2.

J Am Chem Soc. Author manuscript; available in PMC 2009 November 19.

Table 1

^{1}H chemical shifts of heme methyls of cytochrome *c* variants

Protein variant	^{1}H Chemical shift, ppm				Met-orientation[a]	<δ>, ppm	Ref.
	1-CH_3	3-CH_3	5-CH_3	8-CH_3			
(1) Pa *c*-551	26.5	13.2	31.5	16.0	A	21.8	*c*
(2) PaN64V	12.9	25.6	17.7	28.1	B[b]	21.1	*c*
(3) Ne c-552	20.7	21.6	24.9	22.6	(A+B)[b]	22.4	*c*
(4) NeV65	21.9	20.6	26.1	21.9	(A+B) [b]	22.6	*c*
(5) NeN64	10.9	29.3	14.1	29.7	B	21.0	*c*
(6) NeG50N/V65	22.2	20.1	26.4	21.5	A	22.6	*c*
(7) PaN64Q	21.4	25.5	19.2	19.8	(A+B)[b]	21.5	57
(8) PaN50G/V65ins	22.9	15.9	29.3	19.2	A[b]	21.8	*c*
(9) Horse cyt *c*	7.2	31.7	10.2	34.5	B	21.1	61, 77
(10) *B. pasteurii c*-553	14.8	28.8	20.9	29.8	B	23.6	*d* 69
(11) *S. cerevisiae* iso-1	8.0	31.3	11.0	34.8	B	21.3	47
(12) *R. rubrum* c2	10.8	29.9	15.0	33.2	B	22.2	47
(13) *Rh. palustris* c2	12.4	31.1	18.3	36.4	B	24.6	67
(14) *P. ZoBell c*-551	21.2	13.6	30.3	17.6	A	20.7	47
(15) *P. stutzeri c*-551	21.3	13.7	30.5	18.0	A	20.9	47

[a] Assignment of Met orientation based on heme methyl shift order using the relationship described in Ref 47. (A+B) indicates a compressed heme methyl shift pattern, consistent with a mixture of orientations A and B.

[b] Linebroadening is observed, consistent with the presence of Met dynamics.

[c] Shifts measured in this study at 299 K.

[d] Shifts measured at 300 K, pH = 7.5.

Table 2

The *g*-tensor values and the correlation between axial (Δ/ξ) and rhombic (V/ξ) ligand-field parameters, with their saturation trends (*b*, *P*1/2) for Pa *c*-551 and Ne *c*-552 over-expressed forms and mutants derived from the EPR measurements performed at $T = 10 \pm .0.5$ K. Other relevant literature data for similar cytochrome *c* proteins have been included as well

Protein variant	g_{max}	g_{mid}	g_{min}	V/ξ	Δ/ξ	V/Δ	$P_{1/2}$ [b]	b [f]	Ref.
(1) Pa *c*-551	3.20 ± 0.01	2.06 ± 0.02	1.23 ± 0.02	1.28 ± 0.02	3.45 ± 0.03	0.37	44.30 ± 2.86	1.00 ± 0.03	*a*
(2) PaN64V	3.05 ± 0.01	2.23 ± 0.02	1.31 ± 0.03	1.53 ± 0.02	2.80 ± 0.05	0.55	38.10 ± 2.30	1.00 ± 0.04	*a*
(3) Ne *c*-552	3.34	1.87	1.17	1.09	4.45	0.24	42.80 ± 4.20	1.0	*a*, 25
(4) NeV65Δ[c]	3.35 ± 0.01	1.87 ± 0.08	1.14 ± 0.02	1.06 ± 0.05	4.30 ± 0.06	0.25	54.50 ± 2.41	1.0 ± 0.04	*a*
(5) NeN64	3.13 ± 0.01	2.18 ± 0.02	1.20 ± 0.02	1.36 ± 0.02	2.74 ± 0.04	0.50	40.60 ± 2.12	1.0 ± 0.06	*a*
(6) NeG50N/V65Δ[c]	3.34 ± 0.01	1.87 ± 0.10	1.15 ± 0.17	1.08 ± 0.06	4.78 ± 1.70	0.23	-	-	*a*
(7) PaN64Q	3.21 ± 0.01	2.09 ± 0.03	1.15 ± 0.05	1.23 ± 0.03	3.02 ± 0.50	0.41	43.60 ± 3.93	1.00 ± 0.05	*a*
(8) PaN50G/V65ins	3.18 ± 0.01	2.11 ± 0.02	1.26 ± 0.01	1.34 ± 0.02	3.31 ± 0.03	0.40	42.40 ± 3.15	1.00 ± 0.05	*a*
(9) Horse cyt *c*	3.06	2.25	1.25	1.48	2.56	0.58	-	-	
(10) *B. pasteurii c*-553	3.36	1.94	0.98	1.00	3.18	0.31	55.10 ± 4.60	1.0	25
(11) *S. cerevisiae* iso-1[e]	3.06	2.25	1.25	1.48	2.56	0.58	-	-	68
(12) *R. rubrum c*-2	3.17	2.05	1.32d	1.36	3.90	0.35	-	-	68
(13) *Rh. palustris c*-2	3.22	2.07	1.22	1.27	3.38	0.38	-	-	67
(14) *P. ZoBell c*-551	2.97	2.24	~1.40	1.69	2.95	0.57	-	-	66
(15) *P. stutzeri c*-551	2.96	2.27	1.62	2.01	3.86	0.52	-	-	65

[a] This work.

[b] Unit in mW.

[c] *g*-tensor and ligand-field data for the dominant HALS component only.

[d] Calculated using Eq. 3 (See Materials and Methods).

[e] Major component, neutral pH.

[f] Line-shape factor ($b = 1$ Gaussian line, $b = 3$ Lorentzian line). The symbol (ξ) indicates the spin-orbit coupling constant (~400 cm-1).